Huygens' Dipole for Polarization-Controlled Nanoscale Light Routing

Sergey Nechayev,[1,2] Jörg S. Eismann,[1,2] Martin Neugebauer,[1,2] Paweł Woźniak,[1,2] Ankan Bag,[1,2] Gerd Leuchs,[1,2] and Peter Banzer[1,2,*]

[1] *Max Planck Institute for the Science of Light, Staudtstr. 2, D-91058 Erlangen, Germany*
[2] *Institute of Optics, Information and Photonics, University Erlangen-Nuremberg, Staudtstr. 7/B2, D-91058 Erlangen, Germany*

(Dated: February 5, 2019)

Structured illumination allows for satisfying the first Kerker condition of in-phase perpendicular electric and magnetic dipole moments in any isotropic scatterer that supports electric and magnetic dipolar resonances. The induced Huygens' dipole may be utilized for unidirectional coupling to waveguide modes that propagate transverse to the excitation beam. We study two configurations of a Huygens' dipole – longitudinal electric and transverse magnetic dipole moments or vice versa. We experimentally show that only the radially polarized emission of the first and azimuthally polarized emission of the second configuration are directional in the far-field. This polarization selectivity implies that directional excitation of either TM or TE waveguide modes is possible. Applying this concept to a single nanoantenna excited with structured light, we are able to experimentally achieve scattering directivities of around 23 dB and 18 dB in TM and TE modes, respectively. This strong directivity paves the way for tunable polarization-controlled nanoscale light routing and applications in optical metrology, localization microscopy and on-chip optical devices.

PACS numbers: 03.50.De, 42.25.Ja, 42.50.Tx

I. INTRODUCTION

In 1983, Kerker et al. predicted directional antenna-like scattering by magneto-dielectric particles [1] owing to the interference of the excited in-phase perpendicular electric and magnetic dipole moments. Such dipole source was termed Huygens' dipole and it is associated with increased forward\suppressed backward scattering [2, 3]. The prediction of directional scattering under plane-wave illumination, supported by experimental demonstrations [2–4], and multipolar generalized versions of it [5–9] turned out to be seminal in the field of optical antennas [10–14]. Considerable efforts have been made to confine the radiated power by single nano-antennas [15–20] and metasurfaces [21–24] into an even narrower angular range. These directive nano-antennas coupled to single emitters allow for controlling the emission intensity distribution [24–30] and polarization [31–34].

Inducing a Huygens' dipole in a nanoparticle under plane-wave illumination requires that the nanoparticle has equal first order electric a_1 and magnetic b_1 Mie coefficients [1]. Importantly, a dipolar scatterer responds only to the *local* electric and magnetic fields, while Maxwell's equations locally permit *any* configuration of these electromagnetic field vectors [35, 36]. Consequently, structured illumination allows for exciting [37] an arbitrary oriented Huygens' dipole in *any* isotropic dipolar scatterer (assuming $a_1, b_1 \neq 0$) and, hence, unidirectional scattering along *any* axis. The first experimental observation of a Huygens' dipole that emits light directionally transverse to the propagation direction of the excitation beam was reported recently [38, 39] using structured illumination and a Si nanoparticle with $|a_1| \neq |b_1|$, while the relative phase between Mie coefficients $Arg(b_1/a_1) \approx \pi/2$ compensated for the inherent phase of the structured excitation field [40, 41]. The observed phenomena was referred to as "transverse Kerker scattering".

In this communication, we report on an experimental polarization resolved quantitative study of transverse Kerker scattering phenomena using a spatially varying cylindrical polarization basis. We utilize two possible realizations of a Huygens' dipole — an in-phase longitudinal electric and transverse magnetic dipole moments (*i*) and vice versa (*ii*) — excited in a high-refractive index dielectric spherical nanoparticle ($a_1 \neq b_1$) with structured illumination [38, 39]. Employing a spatially varying cylindrical polarization basis, we directly confirm that transversely directional light emission of (*i*) and (*ii*) appears in the radially and azimuthally polarized (TM and TE) components [20], respectively. We obtain transverse scattering asymmetries of approximately 23 dB and 18 dB in radially and azimuthally polarized components of the scattered light and conclude that (*i*) and (*ii*) are capable of directional excitation of TM and TE waveguide modes, respectively. Experimentally achieving these remarkable transverse scattering asymmetries in the specific polarization modes using an individual nanoantenna provides for a route towards tunable polarization-controlled nanoscale light routing for applications in optical metrology and on-chip optical devices.

* peter.banzer@mpl.mpg.de; http://www.mpl.mpg.de/

II. THEORY

We start by briefly describing the excitation of a Huygens' dipole in a Mie scatterer with structured illumination. Consider a radially polarized beam, which is tightly focused by an aplanatic objective with high numerical aperture (NA) [42]. In the vicinity of its geometrical focus the field can be approximated by $\mathbf{E}_{\mathrm{rad}}^{\mathrm{foc}}(x,y,z)\propto\left(x\mathbf{e}_x+y\mathbf{e}_y+\frac{2\imath}{k_{\mathrm{eff}}}\mathbf{e}_z\right)\exp(\imath k_{\mathrm{eff}}z)$ [43, 44], with the Cartesian basis vectors $\mathbf{e}_\zeta$ ($\zeta=x,y,z$) and k_{eff} the effective wavenumber [45]. We employ the Maxwell-Faraday equation for time harmonic electromagentic waves, $\mathbf{H}_{\mathrm{rad}}^{\mathrm{foc}}=\frac{-\imath}{k\eta}\nabla\times\mathbf{E}_{\mathrm{rad}}^{\mathrm{foc}}$, to obtain the focal magnetic field, where k and η are the free-space wavenumber and impedance, respectively. Finally, we obtain the focal fields of a focused azimuthally polarized beam via the electromagnetic duality transformation $\{\mathbf{E},\mathbf{H}\}\rightarrow\{\mathbf{H},-\mathbf{E}\}$. This approach leads to compact approximations of both beams in the focal plane ($z=0$) as follows:

$$\mathbf{E}_{\mathrm{rad}}^{\mathrm{foc}}(x,y)=x\mathbf{e}_x+y\mathbf{e}_y+\frac{2\imath}{k_{\mathrm{eff}}}\mathbf{e}_z, \tag{1}$$

$$\mathbf{H}_{\mathrm{rad}}^{\mathrm{foc}}(x,y)=\frac{k_{\mathrm{eff}}}{k\eta}\left(-y\mathbf{e}_x+x\mathbf{e}_y\right), \tag{2}$$

$$\mathbf{E}_{\mathrm{azi}}^{\mathrm{foc}}(x,y)=y\mathbf{e}_x-x\mathbf{e}_y, \tag{3}$$

$$\mathbf{H}_{\mathrm{azi}}^{\mathrm{foc}}(x,y)=\frac{k_{\mathrm{eff}}}{k\eta}\left(x\mathbf{e}_x+y\mathbf{e}_y+\frac{2\imath}{k_{\mathrm{eff}}}\mathbf{e}_z\right). \tag{4}$$

We notice in Eqs. (1)-(4) that for the radially (azimuthally) polarized beam the longitudinal electric (magnetic) field is $\pm\pi/2$ dephased relatively to transverse magnetic (electric) field [40, 41]. Consequently, as it was discussed in depth in [38, 39], a dipolar Mie scatterer excited at a wavelength such that the Mie coefficients compensate this phase $Arg(b_1/a_1)=\pi/2$ and positioned in the proximity of the optical axis (owing to the cylindrical symmetry we only discuss positions along the x-axis) allows for constructing the Huygens' dipoles (i) and (ii) using a focused radially and azimuthally polarized beam, respectively [38, 39, 46]. Specifically, a radially polarized beam [Eqs. (1)-(2)] excites $\mathbf{p}=-\imath x|a_1|\mathbf{e}_x+\frac{2}{k_{\mathrm{eff}}}|a_1|\mathbf{e}_z\equiv\left(p_x^{\mathrm{rad}},0,p_z^{\mathrm{rad}}\right)$ and $\mathbf{m}/c=\frac{k_{\mathrm{eff}}}{k}x|b_1|\mathbf{e}_y\equiv\left(0,m_y^{\mathrm{rad}}/c,0\right)$ [38, 40, 47], where c is the speed of light in vacuum. Here, p_z^{rad} and m_y^{rad} constitute a Huygens' dipole (i) at the position $x_i=\pm\frac{2|a_1|k}{|b_1|k_{\mathrm{eff}}^2}$ while p_x^{rad} is an unwanted parasitical component, whose contribution is minimized if $|a_1(\lambda)/b_1(\lambda)|\ll1$ [38, 48]. Alternatively, an azimuthally polarized beam [Eqs. (3)-(4)] excites $\mathbf{p}=x|a_1|\mathbf{e}_y\equiv\left(0,p_y^{\mathrm{azi}},0\right)$ and $\mathbf{m}/c=-\imath\frac{k_{\mathrm{eff}}}{k}x|b_1|\mathbf{e}_x+\frac{2}{k}|b_1|\mathbf{e}_z\equiv\left(m_x^{\mathrm{azi}}/c,0,m_z^{\mathrm{azi}}/c\right)$ [39]. In this case, m_z^{azi} and p_y^{azi} constitute a Huygens' dipole (ii) at $x_{ii}=\pm\frac{2|b_1|}{|a_1|k}$, while m_x^{azi} is the unwanted component, whose contribution is minimized if $|a_1(\lambda)/b_1(\lambda)|\gg1$ [39, 48].

To mimic the coupling of the Huygens' dipoles (i) and (ii) to a high-refractive index dielectric waveguide, we assume that the focal plane ($z=0$) constitutes a boundary between two media – air ($z<0$) and dielectric ($z>0$) with a refractive index n. The excited dipoles are positioned in air at distance d above the interface ($z<0$ half-space). The far-field scattered light $\mathbf{E}^{\infty}(k_x,k_y)=\left[\mathrm{E}^{\mathrm{TM}},\mathrm{E}^{\mathrm{TE}}\right]^{\mathrm{T}}$, coupled to the higher-density medium ($z>0$) in TM\TE polarization basis can be written as [43, 49]:

$$\begin{bmatrix}\mathrm{E}_{(i)}^{\mathrm{TM}}\\ \mathrm{E}_{(i)}^{\mathrm{TE}}\end{bmatrix}\propto C\mathbf{F}\begin{bmatrix}\frac{k_xk_z}{k_\perp k}p_x^{\mathrm{rad}}-\frac{k_\perp}{k}p_z^{\mathrm{rad}}+\frac{k_x}{k_\perp}m_y^{\mathrm{rad}}/c\\ -\frac{k_yk_z}{k_\perp k}m_y^{\mathrm{rad}}/c-\frac{k_y}{k_\perp}p_x^{\mathrm{rad}}\end{bmatrix}, \tag{5}$$

$$\begin{bmatrix}\mathrm{E}_{(ii)}^{\mathrm{TM}}\\ \mathrm{E}_{(ii)}^{\mathrm{TE}}\end{bmatrix}\propto C\mathbf{F}\begin{bmatrix}\frac{k_yk_z}{k_\perp k}p_y^{\mathrm{azi}}-\frac{k_y}{k_\perp}m_x^{\mathrm{azi}}/c\\ \frac{k_x}{k_\perp}p_y^{\mathrm{azi}}-\frac{k_xk_z}{k_\perp k}m_x^{\mathrm{azi}}/c+\frac{k_\perp}{k}m_z^{\mathrm{azi}}/c\end{bmatrix}, \tag{6}$$

where $\mathbf{F}=\mathrm{diag}(t_p,t_s)$ is the matrix of the Fresnel transmission coefficients [43], $C=\exp(\imath k_zd)\left(k^2n^2-k_\perp^2\right)^{1/2}/k_z$, $k_\perp=\left(k_x^2+k_y^2\right)^{1/2}\leq nk$ is the transverse wavenumber and $k_z=\left(k^2-k_\perp^2\right)^{1/2}$ has a positive imaginary part $\Im[k_z]\geq0$. Eqs. (5)-(6) show that when neglecting the small transverse dipole components p_x^{rad} and m_x^{azi}, (i) and (ii) can have directionality only in TM and TE polarized emission, respectively.

III. EXPERIMENT

As nanoantenna we choose a concentric core-shell spherical nanoparticle, positioned on a glass substrate ($n=1.52$) using a custom AFM-based pick-and-place method [50], with the core radius of $r_{\mathrm{Si}}=78\,\mathrm{nm}$ made of crystalline silicon [51] and a 6 nm thick shell made of SiO_2 [51]. In Fig. 1 (a), we plot the first and second order free-space Mie coefficients [52, 53] a_1, b_1, a_2, b_2, showing that the scatterer is well characterized by its dipolar response for $\lambda>520\,\mathrm{nm}$. The plot in Fig. 1 (b) shows that $Arg(b_1/a_1)=\pi/2$ at $\lambda_i=620\,\mathrm{nm}$ and $\lambda_{ii}=520\,\mathrm{nm}$, while $|a_1(\lambda_i)/b_1(\lambda_i)|<1$ and $|a_1(\lambda_{ii})/b_1(\lambda_{ii})|>1$ in Fig. 1 (a). Consequently, following our arguments in the previous section and the detailed discussion in [38, 39], λ_i and λ_{ii} satisfy the conditions for the excitation of the Huygens' dipoles (i) and (ii) using focused radially and azimuthally polarized beams, respectively, while the phase delay between the Mie coefficients $Arg(b_1/a_1)=\pi/2$ is compensated by the phase delay of the exciting field components as appears in Eq. (1)- (4).

Our setup [38, 54] is schematically depicted in Fig. 1 (c). We prepare radially and azimuthally polarized beams using a q-plate [55] and spatially filter them [56]. The resulting beams are focused by a high numerical aperture (NA=0.9) objective. The substrate is mounted onto a 3D piezo actuator, allowing for precise positioning of the nanoparticle in the focal plane. The transmitted and scattered light is collected by a confocally aligned index-matched immersion-type objective (NA=1.4). The Fourier space (far-field) of the light emitted by the nanoparticle is obtained in the back fo-

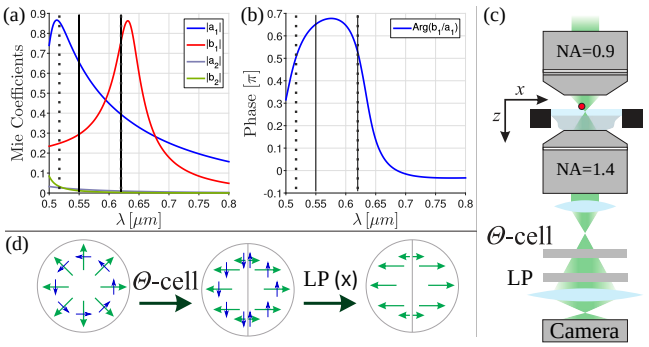

Figure 1. (a) Absolute values of the first and second order Mie coefficients of a core-shell nanoparticle with Si core of radius $r_{\mathrm{Si}}=78\,\mathrm{nm}$ and a SiO_2 shell of thickness 6 nm in free-space. (b) The corresponding phase difference between the first order Mie coefficients. The dotted vertical black lines show the wavelengths $\lambda_i=620\,\mathrm{nm}$ and $\lambda_{ii}=520\,\mathrm{nm}$ where the phase difference is approximately $\pi/2$. The solid vertical black lines show the experimentally found wavelengths $\lambda_i^{\mathrm{exp}}=620\,\mathrm{nm}$ and $\lambda_{ii}^{\mathrm{exp}}=550\,\mathrm{nm}$ that give maximum transverse scattering asymmetry into TM and TE polarized modes, respectively. (c) Experimental setup. An incident radially or azimuthally polarized beam is focused by a high numerical aperture (NA) objective onto the nanoparticle, positioned on a glass substrate, which is actuated by a 3D piezo stage. An immersion-type objective collects the transmitted and scattered light. The back focal plane of the collecting objective is imaged onto the polarization conversion-projection unit and imaged again onto a camera. (d) Schematic presentation of the polarization conversion-projection unit. The Θ-cell converts the impinging TM (radial) and TE (azimuthal) polarizations into linearly polarized Cartesian omponents (x and y), respectively, introducing a π-phase singularity along $x=0$. The intensity distribution in the TM and TE modes can be measured by setting the transmission axis of the subsequent linear polarizer (LP) to x and y, respectively, as shown for x.

cal plane (BFP) of the collecting objective up to the transverse wavenumber $k_\perp/k\leq 1.4$. The angular range $0.9<k_\perp/k\leq 1.4$ corresponds to scattered light only. We image the BFP of the collecting objective onto a polarization conversion-projection unit consisting of a Θ-cell [57] and a rotatable linear polarizer. The Θ-cell converts the TM and TE polarized components into linear Cartesian x and y polarized components, respectively, as illustrated in Fig. 1 (d). The subsequent linear polarizer filters the desired projection. The second lens in Fig. 1 (c) images the BFP and resulting intensity distribution onto a camera.

Experimentally, we record $|\mathrm{E}^{\mathrm{TM}}|^2$ and $|\mathrm{E}^{\mathrm{TE}}|^2$ for radially and azimuthally polarized excitations at various wavelengths and transverse positions of the nanoparticle. We find a maximum transverse scattering asymmetry in the TM mode with radially polarized excitation at a wavelength of $\lambda_i^{\mathrm{exp}}=620\,\mathrm{nm}$ at the position $|x_i^{\mathrm{exp}}|=150\,\mathrm{nm}\pm 5\,\mathrm{nm}$ with expected theoretical values $\lambda_i=620\,\mathrm{nm}$ and $|x_i|=160\,\mathrm{nm}$. For azimuthally polarized excitation the maximal asymmetry in the TE mode is found at $\lambda_{ii}^{\mathrm{exp}}=550\,\mathrm{nm}$ and $|x_{ii}^{\mathrm{exp}}|=75\,\mathrm{nm}\pm 5\,\mathrm{nm}$ with theoretical values $\lambda_{ii}=520\,\mathrm{nm}$ and $|x_{ii}|=78\,\mathrm{nm}$. The deviation from the theoretical values for radially polarized excitation originates from neglecting the reflected incident field in Eqs. (1)-(2), neglecting the transverse electric field in Eq. (1), substrate-induced bi-anisotropy [58, 59] and linear approximation of the focal fields. For azimuthally polarized excitation, even larger deviations are expected owing to the rising quadrupole contributions at shorter wavelengths as seen in Fig. 1 (a). The mentioned effects can be incorporated in the model using a T-matrix approach [39, 60].

In Fig. 2 we plot the obtained polarization resolved BFP images at $\lambda_i^{\mathrm{exp}}=620\,\mathrm{nm}$, $x_i^{\mathrm{exp}}=-150\,\mathrm{nm}$ for radially polarized excitation (a) and at $\lambda_{ii}^{\mathrm{exp}}=550\,\mathrm{nm}$, $x_{ii}^{\mathrm{exp}}=75\,\mathrm{nm}$ for azimuthally polarized excitation (c). Fig. 2 (a), (c) clearly show that the Huygens' dipole configurations (i) and (ii) lead to directional scattering in the TM component only for radial excitation (i) and the TE component only (ii) for azimuthal excitation. Hence, the two configurations are also capable of directionally exciting TM and TE polarized waveguide modes, respectively. The actual transverse scattering asymmetry into a specific polarization mode can be presented by plotting the radiation diagrams. To this end, we evaluate the TE and TM intensity components in the BFP images at the critical angle $k_\perp=k$ using polar plots $\rho\,(\theta)=|\mathrm{E}^{\mathrm{TE\backslash TM}}|^2\,(\theta)$, as shown on the right-hand side of Fig. 2, where ρ is the absolute value of radius vector and $\theta=\tan^{-1}(k_y/k_x)$. We experimentally obtain directivity of approximately 23 dB and 18 dB of coupling of the Huygens' dipoles (i) and (ii) into TM and TE polarized modes, respectively.

Finally, we perform a nonlinear least squares fitting of the experimental BFP images in Fig. 2 (a) and (c) with our model in Eqs. (5) and (6) and summarize the results in Table I. For the wavelength of $\lambda_i^{\mathrm{exp}}=620\,\mathrm{nm}$, we achieve a virtually perfect Huygens' dipole (i) — $p_z^{rad}\approx -m_y^{rad}/c$ with a very significant parasitic component of p_x^{rad}. Nevertheless, p_x^{rad} does not influence transverse scattering asymmetry into the TM polarized mode, since around the critical angle $k_\perp\approx k$ the longitudinal wavenumber $k_z\approx 0$ nullifies the contribution of p_x^{rad}, as appears in the first line of Eq. (5). Moreover, p_x^{rad} also does not influence the transverse scattering asymmetry into the cross-polarized TE mode, since along the scattering direction defined by the k_x-axis we have $k_y\equiv 0$, which nullifies the contribution of p_x^{rad} to the TE mode, as appears in the second line of Eq. (5). For the wavelength of $\lambda_{ii}^{\mathrm{exp}}=550\,\mathrm{nm}$, we achieve a virtually perfect Huygens' dipole (ii) — $p_y^{azi}\approx m_z^{azi}/c$ with a significant parasitic component of m_x^{azi}/c, which, following the same line of arguments as for p_x^{rad}, does not influence the transverse scattering asymmetry. In Fig. 2 (b) and (d) we plot the corresponding theoretical (fitted) BFP images and radiation patterns, using the results shown in Tab. I and Eqs. (5)-(6).

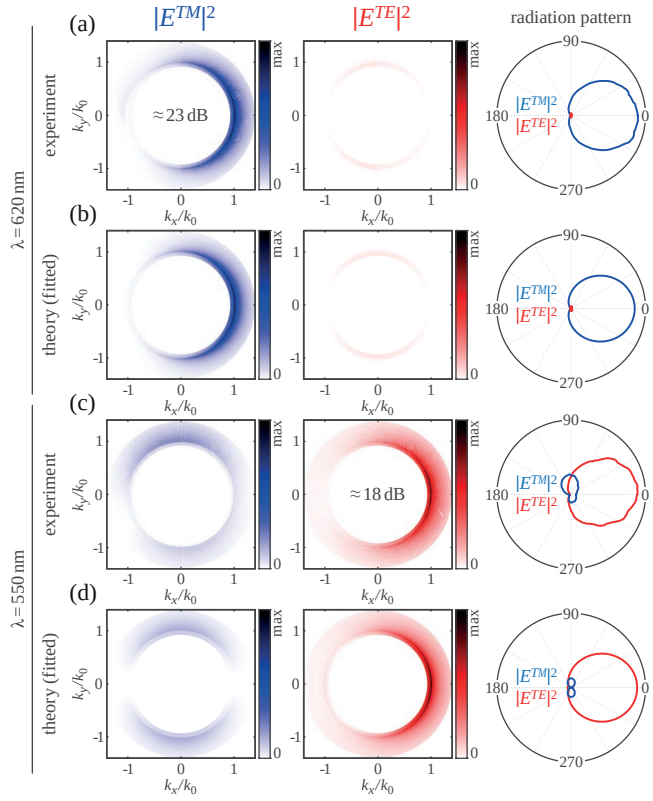

Figure 2. (a) and (c) – polarization resolved measurements of the far-field scattered light. The nanoantenna is positioned in the focal plane of focused radially and azimuthally polarized beams at $\mathbf{r}=(-150\,\mathrm{nm}, 0, 0)$ and $\mathbf{r}=(75\,\mathrm{nm}, 0, 0)$, respectively. The plots show the intensity distribution in TM (radial) and TE (azimuthal) polarized modes in the back focal plane (BFP) of the collecting objective. (b) and (d) – corresponding theoretical (fitted) BFP distributions calculated with Eqs. (5)-(6). The dipole moments used to plot (b) and (d) were obtained by a nonlinear least squares fitting of (a) and (c) with Eqs. (5)-(6). The right column shows the corresponding radiation diagrams – the intensity distribution in the BFP as a function of the polar angle $\theta=\tan^{-1}(k_y/k_x)$.

λ [nm]	p_x	p_y	p_z	m_x/c	m_y/c	m_z/c
620	$0.60e^{\imath 0.51\pi}$	0	1	0	$0.95e^{\imath 0.93\pi}$	0
550	0	$1.05e^{\imath 1.84\pi}$	0	$0.44e^{\imath 1.25\pi}$	0	1

Table I. Summary of the dipole moments retrieved from the experimental BFP data shown in Fig. 2 (a), (c) and fitted with Eqs. (5)-(6).

IV. CONCLUSION

In conclusion, we have experimentally investigated the polarization properties of Huygens' dipoles induced by structured illumination by analyzing their emission properties in cylindrical polarization basis. Utilizing a single nanoantenna excited with structured light, we were able to experimentally achieve transverse scattering asymmetries of around 23 dB and 18 dB in the radial (TM) and azimuthal (TE) polarization mode, respectively. Our scheme may find applications in optical metrology, localization microscopy and on-chip tunable polarization-controlled light routing.

[1] M. Kerker, D.-S. Wang, and C. L. Giles, JOSA **73**, 765 (1983).
[2] J. M. Geffrin, B. García-Cámara, R. Gómez-Medina, P. Albella, L. S. Froufe-Pérez, C. Eyraud, A. Litman, R. Vaillon, F. González, M. Nieto-Vesperinas, J. J. Sáenz, and F. Moreno, Nature Communications **3**, 1171 (2012).
[3] S. Person, M. Jain, Z. Lapin, J. J. Sáenz, G. Wicks, and L. Novotny, Nano Letters **13**, 1806 (2013).
[4] Y. H. Fu, A. I. Kuznetsov, A. E. Miroshnichenko, Y. F. Yu, and B. Luk'yanchuk, Nature Communications **4**, 1527 (2013).
[5] R. Alaee, R. Filter, D. Lehr, F. Lederer, and C. Rockstuhl, Optics Letters **40**, 2645 (2015).
[6] A. Pors, S. K. H. Andersen, and S. I. Bozhevolnyi, Optics Express **23**, 28808 (2015).
[7] L. Wei, N. Bhattacharya, and H. P. Urbach, Optics Letters **42**, 1776 (2017).
[8] W. Liu and Y. S. Kivshar, Opt. Express **26**, 13085 (2018).
[9] S. Kruk and Y. Kivshar, ACS Photonics **4**, 2638 (2017).
[10] P. Mühlschlegel, H.-J. Eisler, O. J. F. Martin, B. Hecht, and D. W. Pohl, Science **308**, 1607 (2005).
[11] P. Bharadwaj, B. Deutsch, and L. Novotny, Advances in Optics and Photonics **1**, 438 (2009).
[12] L. Novotny and N. van Hulst, Nature Photonics **5**, 83 (2011).
[13] A. E. Krasnok, A. E. Miroshnichenko, P. A. Belov, and Y. S. Kivshar, Optics Express **20**, 20599 (2012).
[14] A. E. Krasnok, I. S. Maksymov, A. I. Denisyuk, P. A. Belov, A. E. Miroshnichenko, C. R. Simovski, and Y. S. Kivshar, Physics-Uspekhi **56**, 539 (2013).
[15] M. Nieto-Vesperinas, R. Gomez-Medina, and J. J. Saenz, JOSA A **28**, 54 (2011).
[16] T. Coenen, E. J. R. Vesseur, A. Polman, and A. F. Koenderink, Nano Letters **11**, 3779 (2011).

[17] B. Rolly, B. Stout, and N. Bonod, Optics Express **20**, 20376 (2012).

[18] T. Coenen, F. Bernal Arango, A. Femius Koenderink, and A. Polman, Nature Communications **5**, 3250 (2014).

[19] P. R. Wiecha, A. Cuche, A. Arbouet, C. Girard, G. Colas des Francs, A. Lecestre, G. Larrieu, F. Fournel, V. Larrey, T. Baron, and V. Paillard, ACS Photonics **4**, 2036 (2017).

[20] M. F. Picardi, A. V. Zayats, and F. J. Rodríguez-Fortuño, Physical Review Letters **120**, 117402 (2018).

[21] I. Staude, A. E. Miroshnichenko, M. Decker, N. T. Fofang, S. Liu, E. Gonzales, J. Dominguez, T. S. Luk, D. N. Neshev, I. Brener, and Y. Kivshar, ACS Nano **7**, 7824 (2013).

[22] Decker Manuel, Staude Isabelle, Falkner Matthias, Dominguez Jason, Neshev Dragomir N., Brener Igal, Pertsch Thomas, and Kivshar Yuri S., Advanced Optical Materials **3**, 813 (2015).

[23] D. Arslan, K. E. Chong, A. E. Miroshnichenko, D.-Y. Choi, D. N. Neshev, T. Pertsch, Y. S. Kivshar, and I. Staude, Journal of Physics D: Applied Physics **50**, 434002 (2017).

[24] L. Langguth, A. H. Schokker, K. Guo, and A. F. Koenderink, Physical Review B **92**, 205401 (2015).

[25] H. Gersen, M. F. García-Parajó, L. Novotny, J. A. Veerman, L. Kuipers, and N. F. van Hulst, Physical Review Letters **85**, 5312 (2000).

[26] T. H. Taminiau, F. D. Stefani, F. B. Segerink, and N. F. van Hulst, Nature Photonics **2**, 234 (2008).

[27] T. H. Taminiau, F. D. Stefani, and N. F. v. Hulst, Optics Express **16**, 10858 (2008).

[28] A. G. Curto, G. Volpe, T. H. Taminiau, M. P. Kreuzer, R. Quidant, and N. F. v. Hulst, Science **329**, 930 (2010).

[29] A. G. Curto, T. H. Taminiau, G. Volpe, M. P. Kreuzer, R. Quidant, and N. F. van Hulst, Nature Communications **4**, 1750 (2013).

[30] I. M. Hancu, A. G. Curto, M. Castro-López, M. Kuttge, and N. F. van Hulst, Nano Letters **14**, 166 (2014).

[31] S. S. Kruk, M. Decker, I. Staude, S. Schlecht, M. Greppmair, D. N. Neshev, and Y. S. Kivshar, ACS Photonics **1**, 1218 (2014).

[32] M. Ren, M. Chen, W. Wu, L. Zhang, J. Liu, B. Pi, X. Zhang, Q. Li, S. Fan, and J. Xu, Nano Letters **15**, 2951 (2015).

[33] M. Cotrufo, C. I. Osorio, and A. F. Koenderink, ACS Nano **10**, 3389 (2016).

[34] C. Yan, X. Wang, T. V. Raziman, and O. J. F. Martin, Nano Letters **17**, 2265 (2017).

[35] A. F. Abouraddy and K. C. Toussaint, Phys. Rev. Lett. **96**, 153901 (2006).

[36] N. Yang and A. E. Cohen, The Journal of Physical Chemistry B **115**, 5304 (2011).

[37] P. Woźniak, P. Banzer, and G. Leuchs, Laser & Photonics Reviews **9**, 231 (2015).

[38] M. Neugebauer, P. Woźniak, A. Bag, G. Leuchs, and P. Banzer, Nature Communications **7**, 11286 (2016).

[39] A. Bag, M. Neugebauer, P. Woźniak, G. Leuchs, and P. Banzer, Phys. Rev. Lett. **121**, 193902 (2018).

[40] M. Neugebauer, T. Bauer, P. Banzer, and G. Leuchs, Nano Letters **14**, 2546 (2014).

[41] A. Aiello, P. Banzer, M. Neugebauer, and G. Leuchs, Nature Photonics **9**, 789 (2015).

[42] R. Dorn, S. Quabis, and G. Leuchs, Physical Review Letters **91**, 233901 (2003).

[43] L. Novotny and B. Hecht, *Principles of Nano-Optics* (Cambridge University Press, Cambridge, 2012).

[44] M. Neugebauer, S. Nechayev, M. Vorndran, G. Leuchs, and P. Banzer, Nano Letters **19**, 422 (2019).

[45] k_{eff} depends on the focusing system [43] and is limited by the wavenumber: $0 \leq k_{\text{eff}} \leq k$. In paraxial approximation, $k_{\text{eff}} \approx k$. For the parameters of the focusing system used in our experiment, $k_{\text{eff}} \approx 0.74k$ and $k_{\text{eff}} \approx 0.78k$ for radially and azimuthally polarized illumination, respectively.

[46] The excited electric and magnetic dipole moments in the scatterer are $\mathbf{p} = \varepsilon_0 \alpha_e \mathbf{E}^{\text{foc}}(x)$ and $\mathbf{m} = \alpha_m \mathbf{H}^{\text{foc}}(x)$, where ε_0 is the vacuum permittivity. The electric (α_e) and magnetic (α_m) polarizabilites of the particle are related to the Mie coefficients as $\alpha_e = \left(6\pi\imath/k_1^3\right) a_1$ and $\alpha_m = \left(6\pi\imath/k_1^3\right) b_1$. We omit global amplitude and phase factors.

[47] S. Nechayev, M. Neugebauer, M. Vorndran, G. Leuchs, and P. Banzer, Phys. Rev. Lett. **121**, 243903 (2018).

[48] It should be noted that for the radially (azimuthally) polarized beam only the longitudinal electric (magnetic) field exists on the optical axis, which further fasciliates the minimisation of the parasitic component for $x_i \ll \lambda$ ($x_{ii} \ll \lambda$).

[49] M. Neugebauer, J. S. Eismann, T. Bauer, and P. Banzer, Phys. Rev. X **8**, 021042 (2018).

[50] U. Mick, P. Banzer, S. Christiansen, and G. Leuchs, in *CLEO: 2014* (Optical Society of America, 2014) p. STu1H.1.

[51] E. D. Palik, *Handbook of optical constants of solids* (Orlando Academic Press, Orlando, 1985).

[52] C. F. Bohren and D. R. Huffman, *Absorption and Scattering of Light by Small Particles* (John Wiley & Sons, New York, 1983).

[53] R. L. Hightower and C. B. Richardson, Appl. Opt. **27**, 4850 (1988).

[54] P. Banzer, U. Peschel, S. Quabis, and G. Leuchs, Optics Express **18**, 10905 (2010).

[55] L. Marrucci, C. Manzo, and D. Paparo, Physical Review Letters **96**, 163905 (2006).

[56] E. Karimi, G. Zito, B. Piccirillo, L. Marrucci, and E. Santamato, Optics Letters **32**, 3053 (2007).

[57] M. Stalder and M. Schadt, Optics Letters **21**, 1948 (1996).

[58] M. W. Knight, Y. Wu, J. B. Lassiter, P. Nordlander, and N. J. Halas, Nano Letters **9**, 2188 (2009).

[59] A. E. Miroshnichenko, A. B. Evlyukhin, Y. S. Kivshar, and B. N. Chichkov, ACS Photonics **2**, 1423 (2015).

[60] M. I. Mishchenko, L. D. Travis, and A. A. Lacis, *Scattering, Absorption, and Emission of Light by Small Particles* (Cambridge University Press, Cambridge, 2002).